Available online at www.sciencedirect.com
ScienceDirect
International Journal of Heat and Mass Transfer 51 (2008) 3669–3682
International Journal of HEAT and MASS TRANSFER
www.elsevier.com/locate/ijhmt

Numerical thermal optimization of the configuration of multi-holed clay bricks used for constructing building walls by the finite volume method

L.P. Li, Z.G. Wu, Z.Y. Li, Y.L. He, W.Q. Tao *

School of Energy and Power Engineering, Xi'an Jiaotong University, Xi'an, China

Received 2 March 2007
Available online 21 April 2008

Abstract

A comprehensive numerical study of the equivalent thermal conductivity of a multi-holed clay brick with the size of 240 × 115 × 90 (in mm) has been conducted, and 50 kinds of combination of holes and arrangements are examined. The indoor–outdoor temperature difference varies from 50 °C to 20 °C. The effects of following factors are studied in details: the hole surface radiation, the width-wise and length-wise hole numbers, and the indoor–outdoor temperature difference. The major findings are as follows: (1) the radiation between hole surfaces has some effect on the equivalent thermal conductivity, thus it should be taken into account; (2) the hole number and arrangement affect the thermal conductivity in a rather complicated manner. Analysis shows that depending on the relative importance of natural convection, surface radiation and heat conduction through the clay solid, the thermal conductivity may decrease with the hole number or increase with the hole number and (3) among the 50 kinds of combination, the optimum configuration is found which has five length-wise holes, four width-wise holes and all the holes are from bottom to top in the depth direction of a brick. Its equivalent thermal conductivity is 0.419 W/(m K), which is only 53.1% of solid clay of which it is made, showing great energy-saving possibility if it is adopted in the construction of building wall.

Detailed discussion of the simulated results is conducted and flow field and temperature distributions are also provided for some typical configurations.

Keywords: Multi-holed clay bricks; Equivalent thermal conductivity; Numerical simulation; Conduction; Natural convection; Surface radiation

1. Introduction

Heat transfers caused by conduction, convection and surface radiation which happen simultaneously are often encountered both in nature and in engineering. In the engineering aspect, examples can be listed as the heat transfer in domestic refrigerators [1], in partially open or closed enclosures [2–4], in double glass windows [5] or in heated rooms [6,7]. Such kinds of heat transfer phenomena are often called as multi-mode heat transfer [8]. The particular concern of the multi-mode heat transfer in this paper is put on the heat transfer in the hollow clay bricks which are widely used nowadays for an efficient thermal insulation of buildings. Yet, through the literature search, papers studying heat transfer characteristics in the hollow clay bricks walls is very limited. In [9], natural convection along with surface radiation in conjugated single and double enclosures was studied by 2D numerical simulation. The results indicate that the thermal boundary conditions have important effects on this kind of heat transfer. Lorente et al. [10] paid attention to single vertical hollow brick, using 2D simplified analytical model to calculate heat flux and thermal resistance. Further, the influence of outdoor temperatures on thermal resistance of the walls constructed

* Corresponding author.
E-mail address: wqtao@mail.xjtu.edu.cn (W.Q. Tao).

0017-9310/$ - see front matter © 2008 Published by Elsevier Ltd.
doi:10.1016/j.ijheatmasstransfer.2007.06.008

Nomenclature

A_{w1}	area of inner surface of calculation unit (m^2)
A_{w2}	area of outer surface of calculation unit (m^2)
c_{pf}	specific heat of air (kJ/(kg K))
G	nominal flow rate of cross-section in holes, $G = \int \rho\|u\| dy\, dz$ (kg/m^3)
h_1	convection heat transfer coefficient of inner surface of wall ($W/(m^2 K)$)
h_2	convection heat transfer coefficient of outer surface of wall ($W/(m^2 K)$)
J	radiosity (W/m^2)
L_1	length of calculation unit in x direction (m)
M_1	length of calculation unit in y direction (m)
N_1	length of calculation unit in z direction (m)
p	pressure (Pa)
Pr	Prandtl number
q_r	net radiant heat flux (W/m^2)
Q_{inwall}	total heat transfer rate cross inner surface of wall (W)
$Q_{outwall}$	total heat transfer rate cross outer surface of wall (W)
R_{max}	the largest mass residual in whole computation field
$S_{c,ad,air}$	additional source term of control volume at air side
$S_{c,ad,clay}$	additional source term of control volume at clay side
T	temperature (K)
T_c	reference temperature (K)
T_{f1}	indoor temperature (K)
T_{f2}	environment temperature (K)
T_{w1}	average temperature of inner surface of wall (K)
T_{w2}	average temperature of outer surface of wall (K)
u	velocity component in x direction (m/s)
v	velocity component in y direction (m/s)
w	velocity component in z direction (m/s)
X_{IJ}	view factor
x, y, z	coordinate (m)
λ_s	thermal conductivity of clay (W/(m K))
λ_f	thermal conductivity of air (W/(m K))
$\bar{\lambda}$	equivalent thermal conductivity (W/(m K))
λ_{nat}	equivalent thermal conductivity when radiation neglected (W/(m K))
λ_{rad}	equivalent thermal conductivity when radiation considered (W/(m K))
ε	surface emissivity
ρ	mass density (kg/m^3)
ρ_c	reference mass density (kg/m^3)
ρ_f	mass density of air (kg/m^3)
α	volumetric thermal expansion coefficient (K^{-1})
η	viscosity (kg/(m s))

with different shapes of vertical hollow bricks was investigated with 2D assumption [11].

Recently, in [12] a 2D conjugated simulation of heat transfer in a multi-holed concrete wall was performed by the commercial software FLUENT and the effect of the hole surface radiation was studied. In [13,14], del Coz Díaz et al. conducted a thermal analysis about some kinds of light concrete hollow brick walls by 3D numerical simulation by the finite element method. In fact, heat transfer occurring in hollow brick walls are of 3D in nature because of the way of laying bricks into walls. Besides, the boundary conditions at the inner and outer surfaces of the walls are generally of convective type. Therefore, 3D numerical simulation can describe the heat transfer more accurately especially for the hollow clay bricks with many holes.

Nowadays, hollow clay bricks have been used extensively for constructing building walls because of their advantages of lightening building loads and improving performance of thermal insulation of the building walls. According to their function, the hollow clay bricks are divided into two categories, of which one is mainly used for bearing building loads and the other is for thermal insulation. As indicated, the focus of this paper is put on the latter.

This paper is aimed at thermal optimizing the arrangement of holes of the hollow clay brick sized by $240 \times 115 \times 90$ (mm) via calculating their equivalent thermal conductivity by using 3D numerical simulation. Here the optimization means to find the configuration of the lowest equivalent thermal conductivity. This type of the hollow clay bricks have 240 mm in length, 115 mm in width and 90 mm in height and are widely used in the present building construction in China. The convective boundary conditions are adopted at the inner and outer surfaces of the walls constructed with such hollow clay bricks. The results are of importance for saving energy and reducing clay consumption.

2. Mathematical formulation of the problem

The pictorial view of the computational domain is shown in Fig. 1a. It consists of four pieces of $240 \times 115 \times 90$ hollow clay bricks that have the same exterior size and the same configuration connected by mortar according to the way of laying bricks, forming one unit of the building walls. This computational domain is the smallest unit of the whole building wall which can be regarded as the periodic repeat in both up/down directions and left/right directions. In Fig. 1b, the top and bottom two layers of brick are depicted with holes shown in detail. The presented hole distribution (which will be referred as L5W4H1 later) is only one of the 50 cases numerically studied in this paper. The

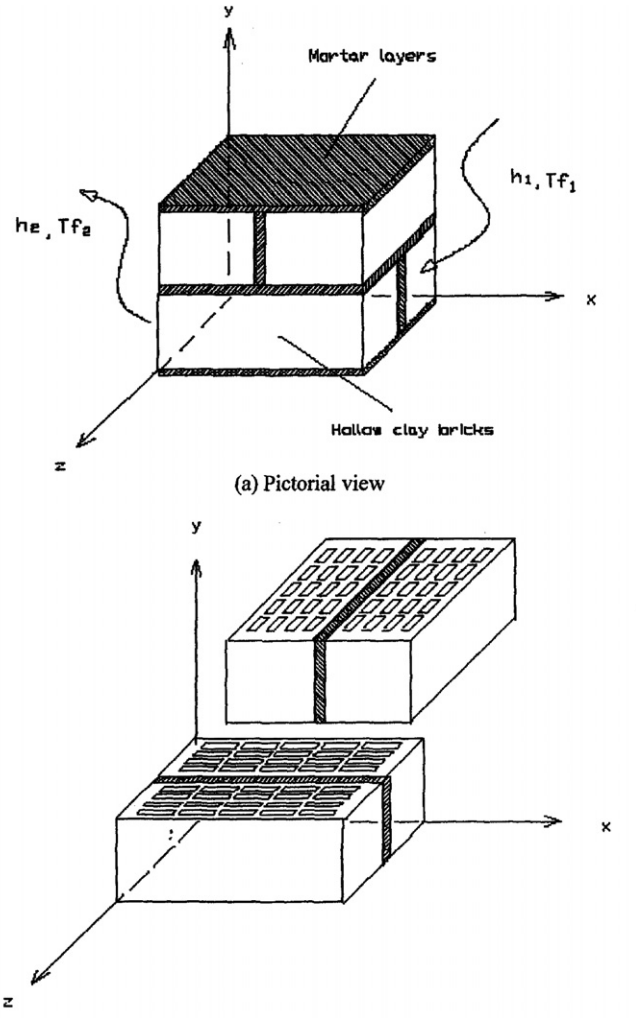

Fig. 1. Computational domain.

principal cross-section of this kind of hollow clay brick is presented in Fig. 2, whose A–A section and B–B section have been shown in Figs. 3 and 4, respectively.

Our preliminary computation results show that the equivalent thermal conductivity depends both on the void fraction and the number of holes. In order to optimize the configuration of the hollow clay brick, the number of holes in both the length-wise and width-wise directions of the brick are varied systematically and 50 kinds of $240 \times 115 \times 90$ hollow clay bricks with different holes and arrangements are finally selected for simulation. These 50 kinds of bricks have one thing in common, i.e., they only have one hole in height, mainly considering the convenience of the process of hollow clay brick production. The hole numbers vary in other two directions: from one to 12 holes in length and one to five holes in width. In these two directions, all the holes are evenly arranged in the sense that the separating spacing between two neighboring holes in the same direction is constant. All of the 50 types of bricks are of the largest void fraction at given hole number. Here the void fraction means the ratio of volume containing air with the total volume of the hollow clay brick. And by the word "largest" we mean that at given hole number and arrangement, the hollow clay brick has its shell of 10 mm thick, the webs separating the holes are in the range of 7.5–10 mm. All the holes have rectangular cross-sections in shape. And the individual cross-section sizes are determined according the above mentioned shell thick and the separating distance.

For the purpose of clarity, we use the symbol of Ln1Wn2Hn3 representing the brick having n1 holes in length, n2 holes in width and n3 holes in height. For example, the symbol L5W4H1 represents the hollow clay brick with 5 holes in length, 4 holes in width and 1 hole in height. The symbols for all kinds of bricks to be simulated are listed in Table 1, in which the void fraction and the total numbers of the holes are also provided. It can be seen from the table that for the given hole number in the width-direction, the void fraction decreases with the increase of hole number in the length-direction. This is because with the increase of hole number the solid separating spacing between two neighboring holes increases.

In the simulation, the following assumptions are adopted: (1) the thermal physical properties of the hollow clay bricks and of the air are constant; (2) flow in it is incompressible, steady state and laminar; (3) air is non-participating medium for radiation; (4) the thermal physical properties of the mortar layers are assumed to be the same as the clay brick; (5) the Boussinesq assumption is valid and (6) except the outer surface and inner surface at which the convective boundary conditions are taken, the other four surfaces of the computational domain are assumed adiabatic.

On the basis of these assumptions, the governing equations describing the problem can be stated as follows [15]:

$$\begin{aligned}
&\frac{\partial(\rho u^2)}{\partial x}+\frac{\partial(\rho uv)}{\partial y}+\frac{\partial(\rho uw)}{\partial z}\\
&\quad=-\frac{\partial p}{\partial x}+\eta\left(\frac{\partial^2 u}{\partial x^2}+\frac{\partial^2 u}{\partial y^2}+\frac{\partial^2 u}{\partial z^2}\right)\\
&\frac{\partial(\rho uv)}{\partial x}+\frac{\partial(\rho v^2)}{\partial y}+\frac{\partial(\rho vw)}{\partial z}\\
&\quad=-\frac{\partial p}{\partial y}+\eta\left(\frac{\partial^2 v}{\partial x^2}+\frac{\partial^2 v}{\partial y^2}+\frac{\partial^2 v}{\partial z^2}\right)+\rho_c g\alpha(T-T_c)\\
&\frac{\partial(\rho uw)}{\partial x}+\frac{\partial(\rho vw)}{\partial y}+\frac{\partial(\rho w^2)}{\partial z}\\
&\quad=-\frac{\partial p}{\partial z}+\eta\left(\frac{\partial^2 w}{\partial x^2}+\frac{\partial^2 w}{\partial y^2}+\frac{\partial^2 w}{\partial z^2}\right)\\
&\frac{\partial(\rho uT)}{\partial x}+\frac{\partial(\rho vT)}{\partial y}+\frac{\partial(\rho wT)}{\partial z}\\
&\quad=\frac{\lambda}{c_p}\left(\frac{\partial^2 T}{\partial x^2}+\frac{\partial^2 T}{\partial y^2}+\frac{\partial^2 T}{\partial z^2}\right)
\end{aligned} \tag{1}$$

where in the light of the relationship of ρ, T, the air expansion coefficient can be expressed as

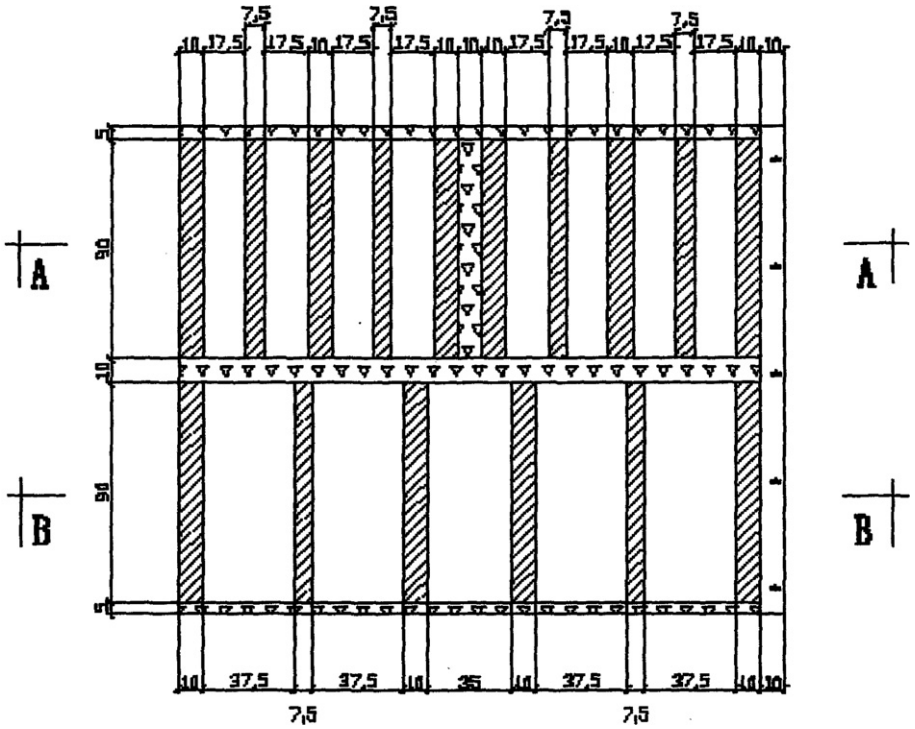

Fig. 2. Principal cross-section for the L5W4H1 hollow clay brick ($z = 0.02$).

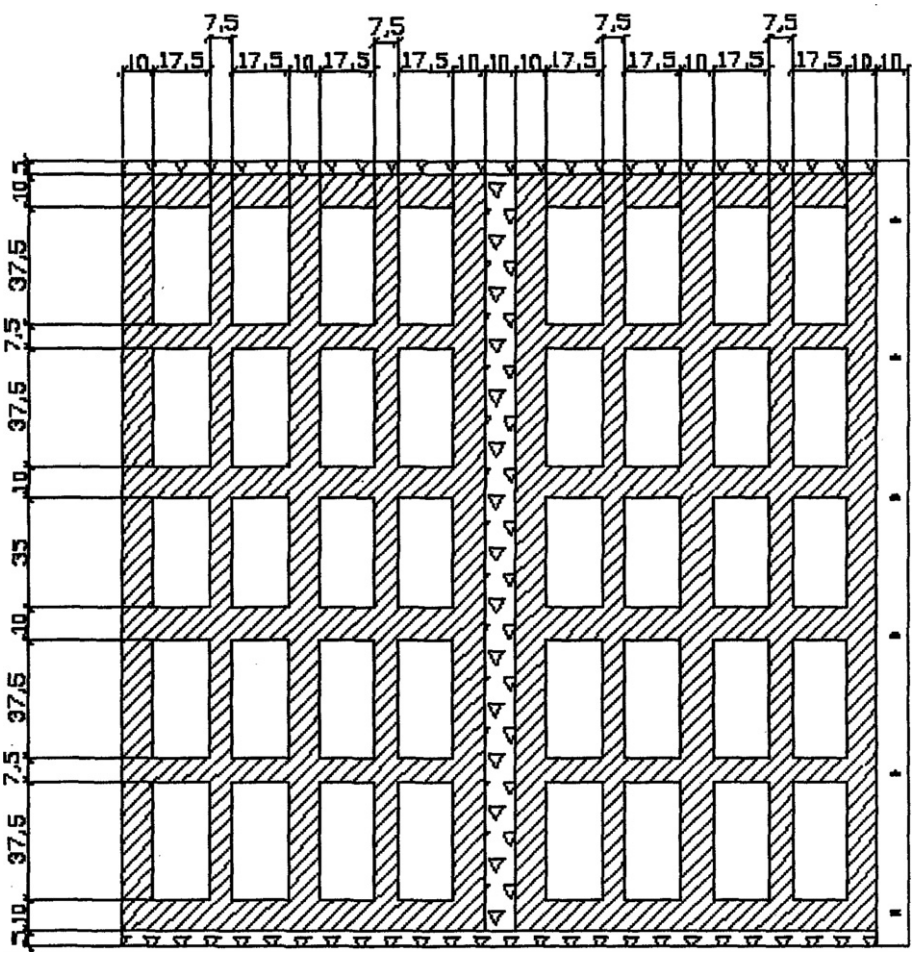

Fig. 3. A–A section for the L5W4H1 hollow clay brick.

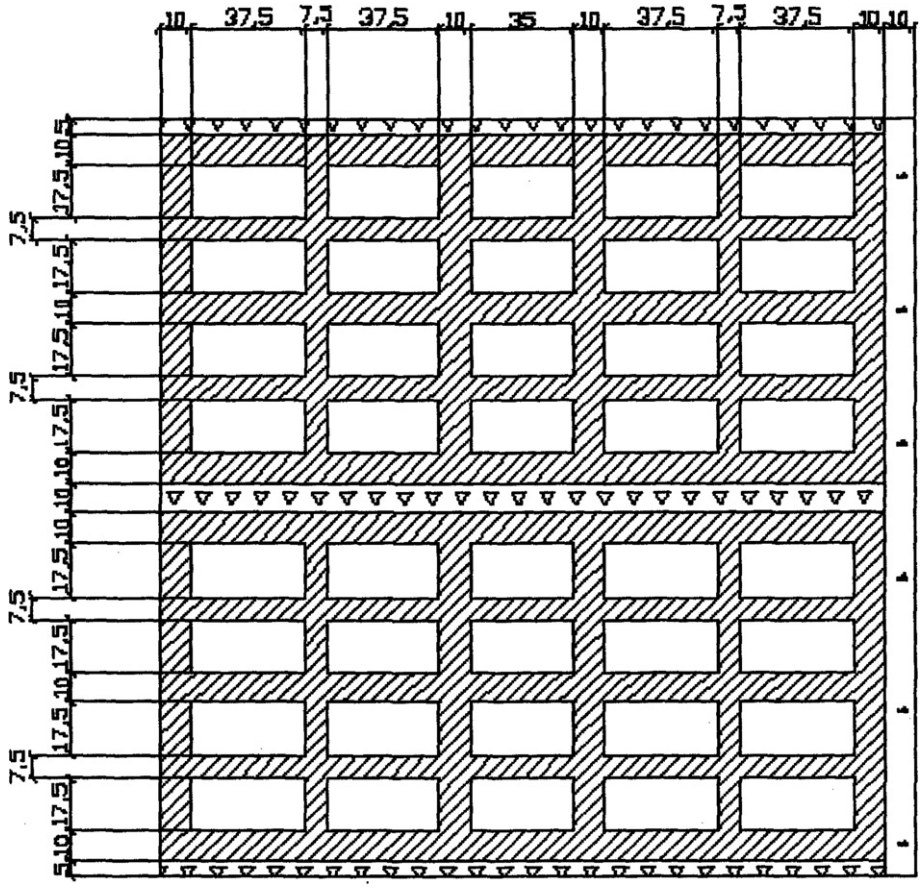

Fig. 4. B–B section for the L5W4H1 hollow clay brick.

$$\alpha = -\frac{1}{\rho}\frac{\partial \rho}{\partial T} \tag{2a}$$

and for the ideal gas we have

$$\alpha = \frac{1}{T} \tag{2b}$$

The boundary conditions are

$$\begin{aligned}
&x = 0, \quad u = v = w = 0, \quad h_2(T_{f2} - T_{w2}) = -\lambda_s \frac{\partial T}{\partial x} \\
&x = L_1, \quad u = v = w = 0, \quad h_1\left(T_{w1} - T_{f1}\right) = -\lambda_s \frac{\partial T}{\partial x} \\
&y = 0, \quad u = v = w = 0, \quad \frac{\partial T}{\partial y} = 0 \\
&y = M_1, \quad u = v = w = 0, \quad \frac{\partial T}{\partial y} = 0 \\
&z = 0, \quad u = v = w = 0, \quad \frac{\partial T}{\partial z} = 0 \\
&z = N_1, \quad u = v = w = 0, \quad \frac{\partial T}{\partial z} = 0
\end{aligned} \tag{3}$$

where L_1, M_1, and N_1 represent the size of the calculation unit in x, y and z direction, respectively. In the following presentation, the surfaces with $x = 0$ and $x = L_1$ will be referred as inner and outer surfaces, respectively.

The thermal physical properties adopted in simulation are as follows

$$\begin{aligned}
&T_{f1} = 293\ \text{K}, \quad T_{f2} = 253\ \text{K}, \quad h_1 = 8.72\ \text{W/(m}^2\ \text{K)}, \\
&h_2 = 23.26\ \text{W/(m}^2\ \text{K)}, \quad Pr = 0.707, \quad c_{pf} = 1005\ \text{J/(kg K)}, \\
&\lambda_f = 0.0244\ \text{W/(m K)}, \quad \eta = 17.2 \times 10^{-6}\ \text{kg/(m s)}, \\
&\rho_f = 1.293\ \text{kg/m}^3, \quad \lambda_s = 0.755\ \text{W/(m K)}, \quad \varepsilon = 0.85
\end{aligned}$$

As indicted above, the thermal physical properties of the mortar layers are assumed to be the same as the clay brick. This is because the average thermal conductivity of the dried mortar does not differ from that of clay brick significantly and their thermal resistance is only a small part of the total one.

3. Numerical simulation method

3.1. General remarks

The above governing equations are discretized by the finite volume method [15]. The discretization scheme for convection term is SGSD which is a stability-guaranteed second-order difference scheme [16] and the pressure–velocity solution algorithm is SIMPLE. TDMA + ADI method is used to solve the discretized algebraic equations in the whole field. The field variables are solved in a conjugated

Table 1
Comparison λ_{nat} with λ_{rad} for 240 × 115 × 90 bricks

Kinds	Holes number	Void fraction (%)	λ_{nat} (W/(m K))	λ_{rad} (W/(m K))	$(\lambda_{rad} - \lambda_{nat})/\lambda_{rad}$ (%)	$e_{thermal\_p}$ $(1/(\lambda_{rad\cdot M})$
L01W1H1	1	75.7	0.599	0.785	23.7	1.172
L02W1H1	2	72.0	0.451	0.591	23.7	1.352
L03W1H1	3	68.8	0.416	0.533	22.0	1.345
L04W1H1	4	65.0	0.408	0.511	20.2	1.251
L05W1H1	5	63.7	0.405	0.494	18.0	1.247
L06W1H1	6	62.0	0.406	0.491	17.3	1.199
L07W1H1	7	60.2	0.407	0.486	16.3	1.156
L08W1H1	8	56.8	0.412	0.485	15.1	1.067
L10W1H1	10	51.6	0.420	0.483	13.0	0.957
L12W1H1	12	46.5	0.426	0.480	11.3	0.871
L01W2H1	2	67.8	0.566	0.708	20.1	0.981
L02W2H1	4	64.7	0.410	0.515	20.4	1.230
L03W2H1	6	61.6	0.372	0.459	19.0	1.269
L04W2H1	8	58.5	0.365	0.439	16.9	1.228
L05W2H1	10	57.0	0.362	0.426	15.0	1.221
L06W2H1	12	55.4	0.363	0.424	14.4	1.183
L07W2H1	14	53.9	0.365	0.421	13.3	1.152
L08W2H1	16	50.8	0.374	0.425	12.0	1.070
L10W2H1	20	46.2	0.388	0.432	10.2	0.962
L12W2H1	24	41.6	0.404	0.441	8.4	0.868
L01W3H1	3	59.8	0.571	0.687	16.9	0.810
L02W3H1	6	57.0	0.414	0.498	16.9	1.044
L03W3H1	9	54.3	0.378	0.446	15.2	1.097
L04W3H1	12	51.6	0.373	0.431	13.5	1.072
L05W3H1	15	50.3	0.372	0.421	11.6	1.069
L06W3H1	18	48.9	0.373	0.421	11.4	1.040
L07W3H1	21	47.6	0.377	0.420	10.2	1.016
L08W3H1	24	44.8	0.389	0.427	8.9	0.949
L10W3H1	30	40.8	0.407	0.440	7.5	0.859
L12W3H1	36	36.7	0.427	0.455	6.2	0.777
L01W4H1	4	55.8	0.557	0.657	15.2	0.770
L02W4H1	8	53.3	0.414	0.486	14.8	0.985
L03W4H1	12	50.7	0.380	0.439	13.4	1.033
L04W4H1	16	48.2	0.377	0.427	11.7	1.011
L05W4H1	20	46.9	0.376	0.419	10.3	1.005
L06W4H1	24	45.7	0.379	0.419	9.5	0.983
L07W4H1	28	44.4	0.384	0.421	8.8	0.955
L08W4H1	32	41.8	0.398	0.430	7.4	0.894
L10W4H1	40	38.0	0.419	0.446	6.1	0.809
L12W4H1	48	34.2	0.441	0.464	5.0	0.733
L01W5H1	5	51.8	0.529	0.618	14.4	0.751
L02W5H1	10	49.5	0.415	0.479	13.4	0.925
L03W5H1	15	47.1	0.386	0.438	11.9	0.965
L04W5H1	20	44.7	0.385	0.428	10.0	0.945
L05W5H1	25	43.6	0.385	0.422	8.8	0.940
L06W5H1	30	42.4	0.389	0.424	8.3	0.916
L07W5H1	35	41.2	0.395	0.427	7.5	0.891
L08W5H1	40	38.9	0.410	0.439	6.6	0.834
L10W5H1	50	35.3	0.433	0.457	5.3	0.756
L12W5H1	60	31.8	0.456	0.474	3.8	0.692

manner [17] in that the field variables in both the solid region and the all isolated holes filled with air are solved simultaneously, and the hole surfaces separating solid and fluid areas become inner parts of the computational domain. To guarantee the continuity of heat flux at the interface the equivalent diffusion coefficient at the separating surfaces should be calculated by the harmonic mean. The values of thermal conductivity are adopted individually for the solid and fluid regions while the specific thermal capacity for the solid region should take the value of fluid [15,17]. The zero velocity of solid region can be obtained by using a very large value of viscosity, say 10^{30}, in the momentum equation. In order to guarantee the convergence of iteration, velocity components and pressure should be relaxed in the iteration procedure. A 3D code has been developed by the authors to implement the above

computations. For the special calculation related to the determination of the equivalent thermal conductivity and surface radiation, the following computational processes have also be included in the code.

3.2. Determination of equivalent thermal conductivity

The thermal insulation performance of the hollow clay bricks is characterized by its equivalent thermal conductivity which can be deduced according to the heat flux equilibrium condition

$$h_1(T_{f1} - T_{w1}) = \frac{\bar{\lambda}}{L_1}(T_{w1} - T_{w2}) = h_2(T_{w2} - T_{f2}) \tag{4}$$

Then

$$\bar{\lambda} = L_1 \cdot h_1 \frac{T_{f1} - T_{w1}}{T_{w1} - T_{w2}} \tag{5}$$

Or

$$\bar{\lambda} = L_1 \cdot h_2 \frac{T_{w2} - T_{f2}}{T_{w1} - T_{w2}} \tag{6}$$

where

$$T_{w1} = \frac{1}{A_{w1}}\left[\sum_{i \in A_{w1}} A(i) \cdot T_w(i)\right] \tag{7a}$$

$$T_{w2} = \frac{1}{A_{w2}}\left[\sum_{i \in A_{w2}} A(i) \cdot T_w(i)\right] \tag{7b}$$

where $T_w(i)$ are the temperatures of the grid points at the inner and outer surfaces of the hollow clay brick walls.

In [13,14], the so-called mass overall thermal efficiency is proposed to evaluate the thermal efficiency of some hollow configuration which is defined as follows:

$$e_{\text{thermal\_}p} = \frac{R_{tot}}{M} = \frac{1}{\lambda_{rad} \cdot M} \tag{8}$$

where R_{tot} is the total thermal resistance and M is the mass of the multi-holed clay brick. This parameter is also determined in our computations.

3.3. Iterative determination of hole surface radiation

As indicated above in the process studied, conduction, convection and radiation occur simultaneously at the interfaces. The interface temperature of the hole is not specified in priori, rather, it is determined during the computation process. Thus the surface radiation affects the temperature field. One unique feature of the present work is the iterative determination of the hole surface radiation. Since each hole has its specific thermal conditions, the surface radiation of all the holes should be simultaneous simulated, making this paper quite unique. Each hole is a cubic with six surfaces, whose temperatures are determined individually during the simulation. The hole number varies from one to 60 for the 50 cases studied. The radiant heat flux at each inner surface of a hole is dealt with as additional source term in the control volumes neighboring with the inner surfaces [9,15]. The additional source term is determined as follows:

For the control volumes at the air side (see Fig. 5)

$$S_{c,ad,air} = -\frac{q_r \delta x_w^+/\lambda_s}{\delta x_w^+/\lambda_s + \delta x_w^-/\lambda_f} \cdot \frac{1}{\Delta x^-} \tag{9a}$$

For the control volumes at the clay side

$$S_{c,ad,clay} = -\frac{q_r \delta x_w^-/\lambda_f}{\delta x_w^+/\lambda_s + \delta x_w^-/\lambda_f} \cdot \frac{1}{\Delta x^+} \tag{9b}$$

where q_r is the net radiant heat flux at the inner surfaces of the holes in the hollow clay bricks. Every hole in the brick has six surfaces and the six surfaces composed of a radiative enclosure. When the enclosure surfaces are presumed gray, diffuse and their temperatures are specified, $q_r(I)$ of surface I can be calculated using the following expressions

$$\begin{aligned} q_r(I) &= \frac{\varepsilon(I)}{1-\varepsilon(I)}\left[C_0\left(\frac{T(I)}{100}\right)^4 - J(I)\right] \\ J(I) &= C_0\varepsilon(I)\left(\frac{T(I)}{100}\right)^4 + (1-\varepsilon(I))\sum_J X_{IJ}J(J) \end{aligned} \tag{10}$$

where the dummy variable $I = 1, 2, 3, 4, 5, 6$ in the temperature term and $J = 1, 2, 3, 4, 5, 6$ in the angle factor (view factor) term; $T(I)$ is the average temperature of surface I of the hole. It should be noted that for each surface of a hole, there are several control volume interfaces and the specific number depends on the hole size. From heat transfer this temperature can be determined by two ways:

$$T(I)^4 = \frac{1}{A(I)}\left[\sum_{i \in I} A(i) \cdot T(i)^4\right] \tag{11}$$

by which the radiant heat flux equilibrium at every radiating surface can be satisfied.

Or

$$T(I) = \frac{1}{A(I)}\left[\sum_{i \in I} A(i) \cdot T(i)\right] \tag{12}$$

by which the convective heat flux equilibrium near every radiating surface can be satisfied.

In Eqs. (11) and (12), the expression $i \in I$ represents all the grids belonging to the I surface. The dummy variable

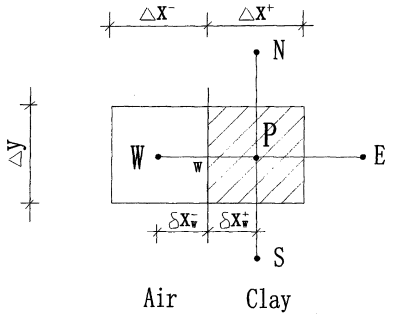

Fig. 5. The control volumes at the sides of w surface.

i represents the control volume interfaces within surface I of a hole and its variation range depends on the case studied.

In fact, $T(I)$ should satisfy both of above heat flux equilibrium. Our numerical practices have shown that it does not matter to chose which one to calculate $T(I)$ because using either of them can obtain identical results. However, using Eq. (12) can have a faster convergence rate. Because in Eq. (12) there is no need to calculate the fourth power of temperature.

In Eqs. (11) and (12), $T(i)$ is the grid temperatures of the hole surface, which varies from iteration to iteration and can be obtained by the interpolation from neighboring grid points according to the heat flux continuity. For example, the temperature of w-interface in Fig. 5 can be calculated by the following equation

$$T(i) = T_w = \frac{T_p\lambda_s/\delta x_w^+ + T_w\lambda_f/\delta x_w^- - q_r(I)}{\lambda_s/\delta x_w^+ + \lambda_f/\delta x_w^-} \tag{13}$$

The angle factor X_{IJ} in Eq. (10) can be calculated by following equation [8]:

For aligned parallel rectangles

$$X_{IJ} = \frac{2}{\pi\overline{X}\overline{Z}}\left\{ In\left[\frac{(1+\overline{X}^2)(1+\overline{Z}^2)}{1+\overline{X}^2+\overline{Z}^2}\right]^{1/2} + \overline{X}(1+\overline{Z}^2)^{1/2}\tan^{-1}\frac{\overline{X}}{(1+\overline{Z}^2)^{1/2}} + \overline{Z}(1+\overline{X}^2)^{1/2}\tan^{-1}\frac{\overline{Z}}{(1+\overline{X}^2)^{1/2}} - \overline{X}\tan^{-1}\overline{X} - \overline{Z}\tan^{-1}\overline{Z}\right\} \tag{14}$$

For perpendicular rectangles with a common edge

$$X_{IJ} = \frac{1}{\pi\overline{X}}\left(\overline{X}\tan^{-1}\frac{1}{\overline{X}} + \overline{Y}\tan^{-1}\frac{1}{\overline{Y}} - (\overline{Y}^2+\overline{X}^2)^{1/2}\tan^{-1}\frac{1}{(\overline{Y}^2+\overline{X}^2)^{1/2}} + \frac{1}{4}In\left\{\frac{(1+\overline{X}^2)}{1+\overline{X}^2+\overline{Y}^2}\left[\frac{\overline{X}^2(1+\overline{X}^2+\overline{Y}^2)}{(1+\overline{X}^2)(\overline{X}^2+\overline{Y}^2)}\right]^{\overline{X}^2} \times \left[\frac{\overline{Y}^2(1+\overline{Y}^2+\overline{X}^2)}{(1+\overline{Y}^2)(\overline{Y}^2+\overline{X}^2)}\right]^{\overline{Y}^2}\right\}\right) \tag{15}$$

Both $T(I)$ and $q_r(I)$ should be iteratively determined during the solution process.

3.4. Convergence condition and grid-independence validation

Convergence criteria of the iteration solution procedure are

$$R_{smax}/G < 10^{-6};$$

$$|Q_{inwall} - Q_{outwall}|/\min(Q_{inwall}, Q_{outwall}) < 10^{-2}$$

$$\text{and} \quad \left|\frac{\bar{\lambda}^{k+300} - \bar{\lambda}^{k}}{\bar{\lambda}^{k+300}}\right| \leqslant 10^{-6}$$

In our preliminary computation, grid-independence of the solution has been examined for the most complex L12W5H1 hollow clay brick in which radiant heat transfer within hole has been considered. Four sets of the grid number have been tested: $102\times82\times102$, $202\times82\times102$, $202\times82\times202$ and $202\times162\times202$. The results of the equivalent thermal conductivity are drawn in Fig. 6.

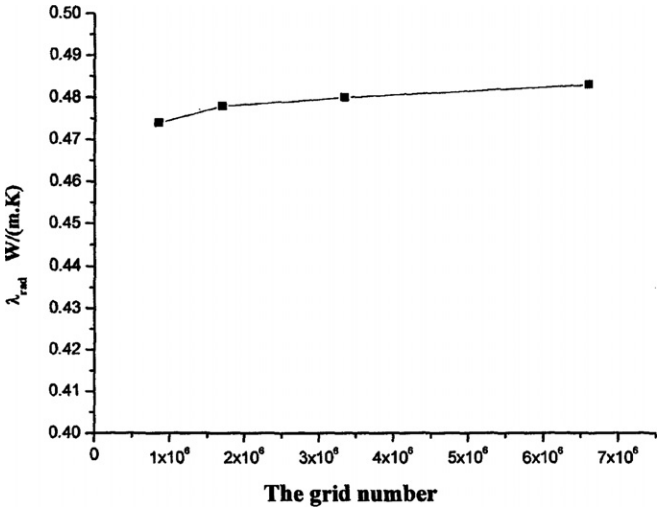

Fig. 6. The validation of grid-independence.

Comparing case 1 with case 4 in Fig. 6, we can observed that increasing the grid number by seven times only leads to no more than 2% difference in the equivalent thermal conductivity. In order to save calculation time, we chose the grid number of case 1 ($L_1 = 102$, $M_1 = 82$ and $N_1 = 102$) in the subsequent simulations for all kinds of $240\times115\times90$ hollow clay bricks. In this set of the grid number, there are at least 720 control volumes in the smallest holes of the hollow clay bricks.

The personal computer used is AMD 3000+ having CPU 1.8 GHZ and EMS memory 1 GB. The total number of iterations and computation times vary from case to case, ranging from about 4000 to 10,000 times and 24–48 h, respectively.

4. Analysis of results

A comprehensive numerical study has been conducted to investigate the effects on the equivalent thermal conductivity of the brick from following factors: the void fraction and the hole number, the hole surface radiation, and the indoor–outdoor temperature difference. In the following presentation, the results of theses effects will first be presented in order, followed by the velocity and temperature distributions of some typical cases. Finally some conclusions will be drawn.

4.1. The relationship between the equivalent thermal conductivity and void fraction as well as the number of holes in the hollow clay bricks

Simulations were first conducted for the cases neglecting the surface radiation heat transfer in holes with a temperature difference between indoor air and outdoor air of $T_{f1} - T_{f2} = 40$ °C, and the predicted results of λ_{nat} for 50

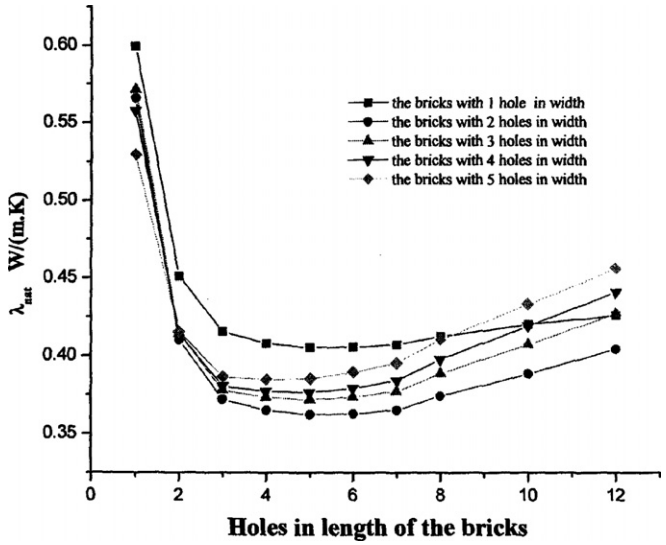

Fig. 7. λ_{nat} for the 240 × 115 × 90 hollow clay bricks.

kinds of 240 × 115 × 90 hollow clay bricks with different holes and arrangement are shown in Fig. 7 and Table 1. In the figure, the ordinate is the number of holes in the length-direction, and the parameter shown in figure is the hole number in the width-direction with fixed size. From this graph we can see that at the fixed number of holes in the width-direction with the increase of the hole number in length, the values of λ_{nat} decrease rapidly from one hole to two holes and three holes, at about 4–5 holes the equivalent thermal conductivity reaches its minimum, and then increases mildly with the increase in hole number in different extent, depending on the hole number in width. Such a variation pattern can be understood as follows.

The equivalent thermal conductivity depends on the combined effect of the heat conduction through the solids and natural convection within the enclosure. Taking the series of one hole in width as an example. When there is only one hole in the length-direction (L1W1H1), the resulting natural convection in the enclosure is rather similar to the one in a two-dimensional cavity with its two side walls at hot and cold temperatures, respectively. The large spacing in the length-direction give an enough space for the natural convection to be fully developed. Thus although the void fraction of this case is the largest, the intensive air natural convection within the closure makes its heat transfer the largest. When the hole number in the length-direction increases to two (L2W1H1), the width–length cross-section of the two enclosures are almost square in shape, and the natural convection is of three-dimensional in nature in which the heat transfer between the hot and cold walls will not so strong as that in the case of L1W1H1. Even though the increase in the solid region of separating spacing increases the cross-section area for heat conduction, it probably can not compensate the reduction in natural convection, leading to a reduction of total heat transfer. This trend holds until to the case of L5W1H1. With the further increase in holes, the effect of increased heat conduction area will be gradually dominated, leading to the increase of equivalent thermal conductivity with the hole number.

Qualitatively, the above discussion can be applied to the other four series shown in Fig. 7. One feature may be noted is that at the same hole number in the length-direction except the cases of only one hole in length, the thermal conductivity first decreases with the hole number in the width-direction and then increases. This variation pattern may also be attributed to the combined effects of the deteriorated natural convection and enhanced heat conduction with the increase of width-wise hole number. When this hole number increases from one to two, the reduced natural convection effect is larger than the enhanced heat conduction from the increase in the separating spacing; while the further increase in the width-wise hole number makes the enhanced heat conduction from the increased separating solid space predominated, hence the thermal conductivity increases again.

From the 50 kinds of bricks, the case of L05W2H1 has the lowest equivalent thermal conductivity of 0.362 W/(m K) at the given conditions simulated.

4.2. The effect of radiation heat transfer on the equivalent thermal conductivity

The predicted thermal conductivities for the 50 kinds of bricks with thermal radiation between hole surfaces being taken into account are shown in Fig. 8 and Table 1. Qualitatively speaking, it can be seen that the variation patterns of the five curves are more or less the same as those without surface radiation. Quantitatively, by carefully inspecting the figure and the table, following features may be noted. First, at the same other conductions, the thermal conductivity with surface radiation is larger than that without thermal radiation, and this is expected from basic heat transfer theory. The largest difference occurs at cases of

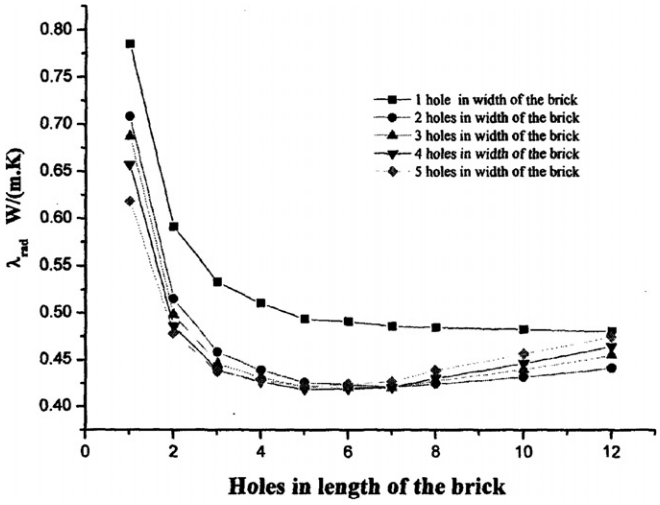

Fig. 8. λ_{rad} for the 240 × 115 × 90 hollow clay bricks.

L1W1H1 and L2W1H1, where 23.7% increase in thermal conductivity is resulted by the thermal radiation (according to the definition of the relative enhancement given in the table). The smallest difference happens at the case of L12W5H1, for which the case with radiation only 3.8% larger than that neglecting surface radiation. Second, as indicated above with the increase in width-wise hole number the increase extent of the thermal conductivity because of radiation decreases. This is because that the increase in width-wise hole number increases the separating walls between width-wise neighboring enclosures, which serves as the thermal radiation shields between the hot and cold surfaces. Thus the increase extent is gradually decreased with the increase in width-wise hole number. Third, from Fig. 8 it can be observed that the series with width-wise 2–5 holes has quite similar thermal performance in that the difference between different width-wise hole number reduces. This means that at given length-wise hole number, changing the width-wise hole number from 2 to 5 has only small effect on the thermal conductivity. When the length-wise hole number is less than 4, the increase in width-wise hole number decreases the thermal conductivity a bit, while when the length-wise hole number is larger than 4, the thermal conductivity has the tendency of first decrease and then increase with the increase in width-wise hole number. Such kind of complicated variation character depends on the competence between following three conflicted factors: increase in width-wise hole will deteriorate the natural convection, increase in the radiation resistance and increase in the thermal conduction area. When the length-wise hole number is less than 4, the first two factors dominate while for larger length-wise hole number the third factor plays a more and more dominated role.

When radiation is taken into account, at the given conditions simulated the smallest equivalent thermal conductivity is 0.419 W/(m K) (L05W4H1) which is 10.3% higher than that neglecting surface radiation for the same configuration. The case of L05W4H1 thus can be regarded as the optimum configuration among the 50 kinds of bricks.

From above comparison study it can be found that generally speaking radiation at hole surface takes a role in the equivalent thermal conductivity and should be taken into account. Thus in the following the results presented include the radiation effect.

In Table 1, the mass overall thermal efficiency defined by Eq. (8) is also listed for the 50 cases (see the last column). It can be found that for the present multi-holed clay brick the variation characteristics of this parameter is not consistent with that of the equivalent thermal conductivity. The largest value of the mass overall thermal efficiency (1.352) occurs for the case of L02W1H1, whose equivalent thermal conductivity is 0.591 W/(m K) and much higher than the smallest value of 0.419 W/(m K). Therefore, as far as the thermal insulation is concerned, this parameter is not appropriate to describe the thermal performance of the multi-holed clay bricks.

4.3. The influence of temperature difference between indoor and outdoor on the equivalent thermal conductivity

For the need of engineering design, the influence of indoor–outdoor temperature difference on λ_{nad} has also been investigated for the most kinds of the hollow clay bricks. The environment temperature is varied from −30 °C to 0 °C, which covers almost all outdoor design temperatures in winter for different provinces and cities in China, while indoor is kept at temperature at 20 °C. The simulation results of the thermal conductivity are listed in Table 2.

From this table, we can see that generally speaking the increase in the indoor–outdoor temperature difference has a positive effect of the value of λ_{rad}, and this is an expected result from heat transfer theory. However, as far as the quantitative effect is concerned, the effect is quite limited. At the simulation range studied, the maximum difference happens for the case of L1W5H1, for which λ_{rad} is 10.7% less at the condition of $T_{f1} - T_{f2} = 20$ °C compared with $T_{f1} - T_{f2} = 40$ °C. For most cases, the change of λ_{rad} is no more than 5%. It is interesting to note that for the optimum configuration as L5W4H1, its thermal conductivity value has hardly change with the indoor–outdoor temperatures temperature difference, as its values are all within

Table 2
The influence of temperature influence on λ_{rad} for 240 × 115 × 90 bricks

Kinds	λ_{rad} (W/(m K)), $T_{f1} - T_{f2}$				Difference (compared with $T_{f1} - T_{f2} = 40$ °C) (%)
	50 °C	40 °C	30 °C	20 °C	
L01W1H1	0.799	0.785	0.769	0.747	1.8 to −4.8
L02W1H1	0.599	0.591	0.581	0.568	1.4 to −3.9
L03W1H1	0.539	0.533	0.526	0.516	1.1 to −3.2
L05W1H1	0.500	0.494	0.487	0.477	1.2 to −3.4
L10W1H1	0.490	0.483	0.475	0.464	1.4 to −3.9
L12W1H1	0.488	0.480	0.471	0.460	1.7 to −4.2
L01W2H1	0.721	0.708	0.693	0.671	1.8 to −5.2
L02W2H1	0.521	0.515	0.508	0.497	1.2 to −3.5
L05W2H1	0.427	0.426	0.424	0.421	0.2 to −1.2
L10W2H1	0.433	0.432	0.431	0.429	0.2 to −0.7
L12W2H1	0.442	0.441	0.440	0.440	0.2 to −0.2
L01W3H1	0.703	0.687	0.666	0.636	2.3 to −7.4
L02W3H1	0.505	0.498	0.489	0.478	1.4 to −4.0
L05W3H1	0.422	0.421	0.420	0.418	0.2 to −0.7
L10W3H1	0.439	0.440	0.441	0.442	−0.2 to 0.5
L12W3H1	0.454	0.455	0.456	0.458	−0.2 to 0.7
L01W4H1	0.679	0.657	0.630	0.595	3.3 to −9.4
L02W4H1	0.494	0.486	0.477	0.466	1.6 to −4.1
L05W4H1	0.419	0.419	0.418	0.417	0.0 to −0.5
L10W4H1	0.445	0.446	0.448	0.450	−0.2 to 0.9
L12W4H1	0.463	0.464	0.466	0.467	−0.2 to 0.6
L01W5H1	0.643	0.618	0.589	0.552	4.0 to −10.7
L02W5H1	0.487	0.479	0.469	0.456	1.7 to −4.8
L03W5H1	0.441	0.438	0.434	0.429	0.7 to −2.1
L05W5H1	0.422	0.422	0.422	0.422	0.0 to 0.0
L10W5H1	0.455	0.457	0.458	0.460	−0.4 to 0.7
L12W5H1	0.474	0.474	0.477	0.479	0.0 to 1.1

0.417–0.419 W/(m K). And the closer the configuration to the optimum, the smaller the change of λ_{rad} with the temperature difference.

4.4. Temperature and velocity distribution for some typical cross-sections of hollow clay bricks

Three kinds of hollow clay bricks, i.e., L01W1H1, L05W4H1 and L12W5H1, are picked out, whose temperature and velocity distribution at some cross-sections ($z = 0.02$ and $z = 0.21$) are shown in Figs. 9–17. All these figures are obtained under the indoor–outdoor temperature difference of 40 °C.

Figs. 9 and 10 show the isotherms at $z = 0.02$ and $z = 0.21$ cross-sections for the L1W1H1 hollow clay brick, respectively. Fig. 11 shows the velocity vectors at the same cross-sections.

Figs. 12–14 illustrate similar temperature and velocity distribution for the L5W4H1 hollow clay brick. Figs. 15–17 are for the L12W5H1 hollow clay brick.

By carefully inspecting these figures, following features may be noted. First, from Figs. 11, 14 and 17 it can be seen that in the x–y cross-section natural convective flows exist moving from right hot surface to left cold surfaces which more or less resemble to those of the benchmark problem in computational heat transfer [15,18]. With the increase in hole number such natural convection is deteriorated, as can be clearly observed from the reduction of velocity

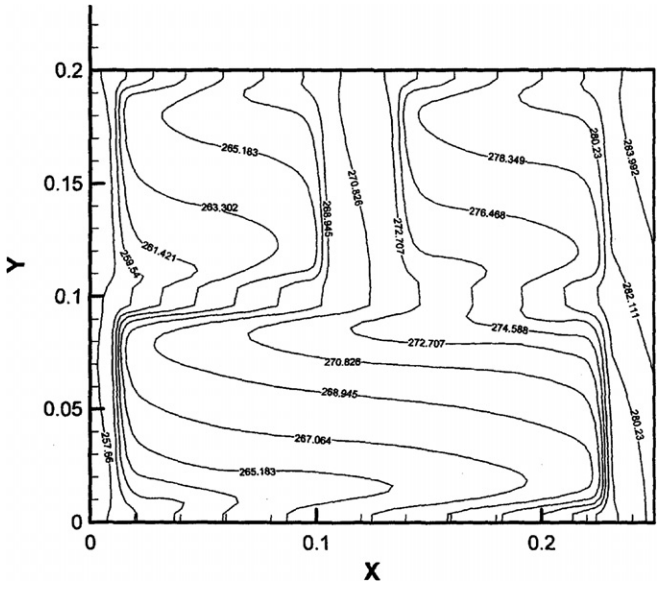

Fig. 9. Isotherms for the L1W1H1 hollow clay brick ($z = 0.02$).

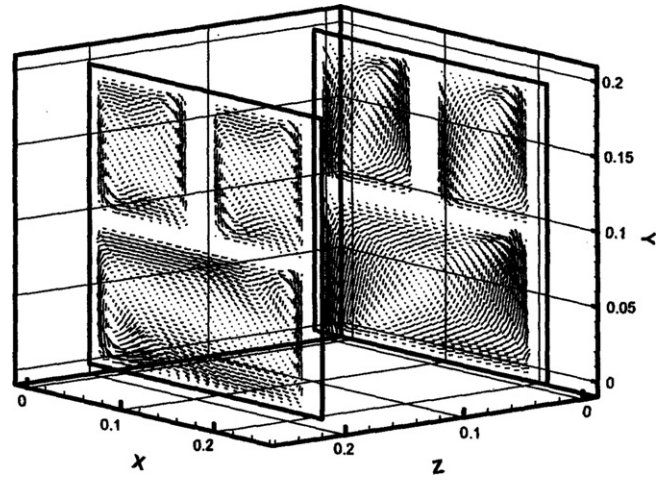

Fig. 11. V vectors for the L1W1H1 hollow clay brick ($z = 0.02$ and $z = 0.21$).

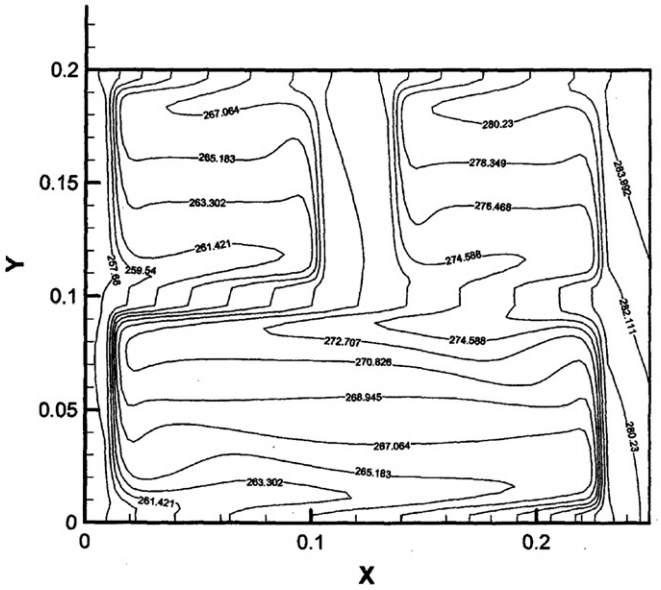

Fig. 10. Isotherms for the L1W1H1 hollow clay brick ($z = 0.21$).

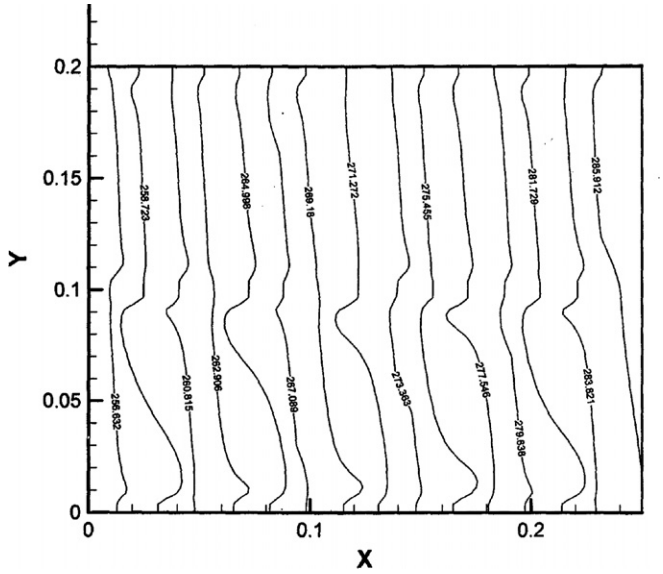

Fig. 12. Isotherms for the L5W4H1 hollow clay brick ($z = 0.02$).

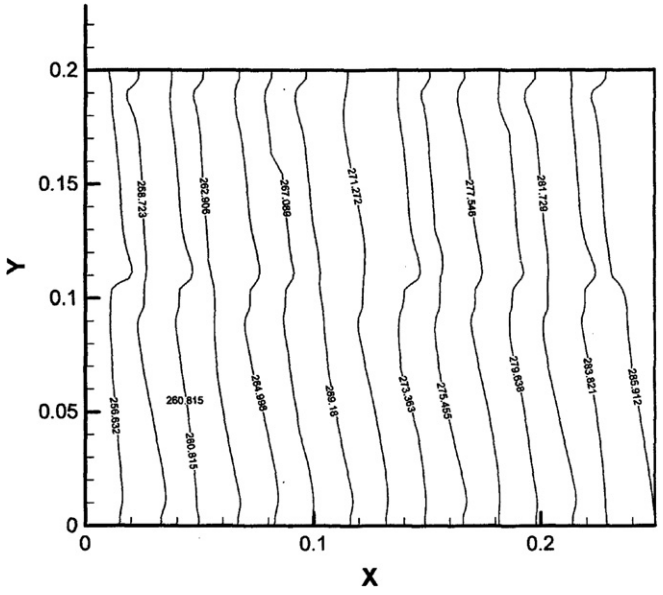

Fig. 13. Isotherms for the L5W4H1 hollow clay brick ($z = 0.21$).

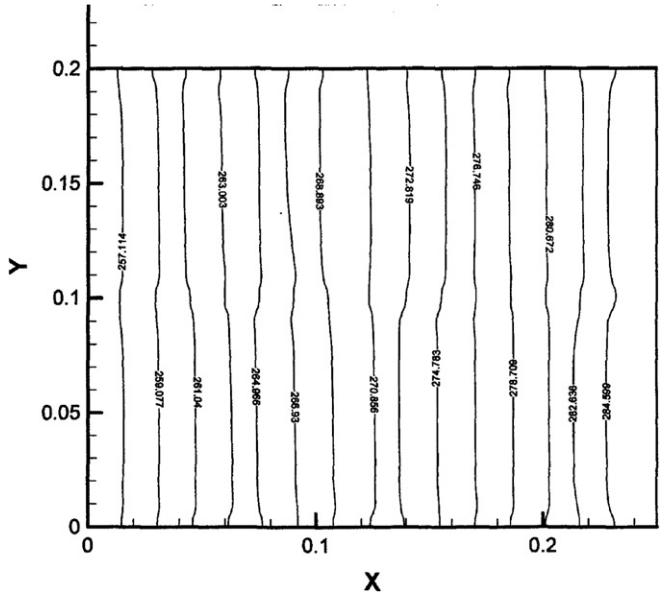

Fig. 15. Isotherms for the L12W5H1 hollow clay brick ($z = 0.02$).

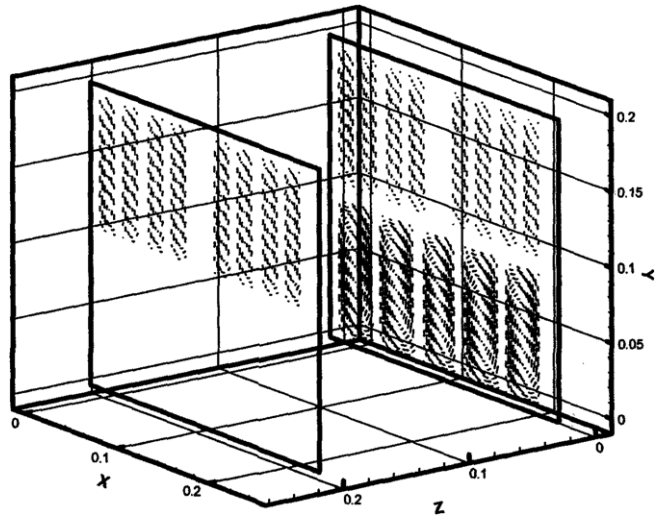

Fig. 14. **V** vectors for the L5W4H1 hollow clay brick ($z = 0.02$ and $z = 0.21$).

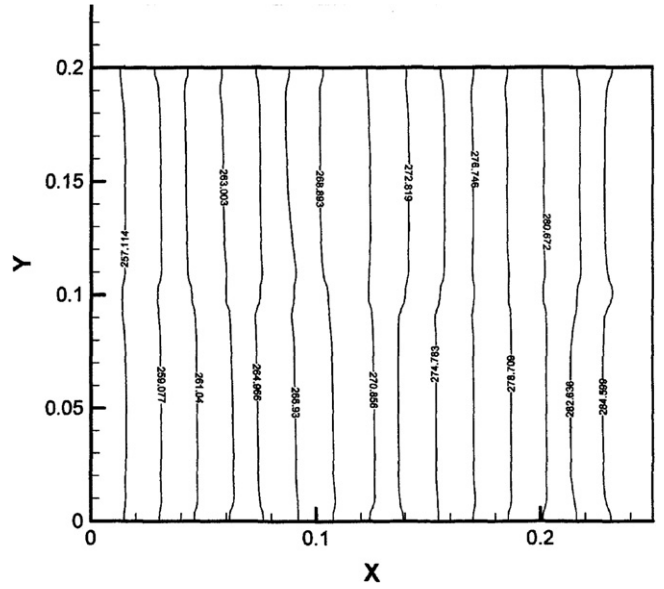

Fig. 16. Isotherms for the L12W5H1 hollow clay brick ($z = 0.21$).

vectors. Second, from Figs. 9, 12 and 15 or 10, 13 and 16, it can be concluded that with the increase in hole number the air temperature distribution gradually approaches the pattern of the pure heat conduction characterized by a series of more or less parallel isothermals, and this variation trend is very consistent with the character of velocity variation with the hole number. The isothermal distributions at two cross-sections for the configuration of L12W5H1 are very like a pure heat conduction within an enclosure with two vertical isothermal walls and adiabatic top/bottom.

This finding illustrates once more that when the hole number of the hollow clay bricks is increased, natural convection and radiation heat transfer in the holes are really decreased. Yet, in order to form those holes more webs (i.e., separating walls) which are made of clay must be placed, leading to some increase in heat conduction through the webs. Therefore, as indicated above with the increase of hole number the final heat transfer performance between the inner and out surfaces depends which factor is dominated.

5. Conclusions

In this work, a comprehensive study on the heat transfer performance of multi-holed clay brick with size of $240 \times 115 \times 90$ has been performed for 50 kinds of hole

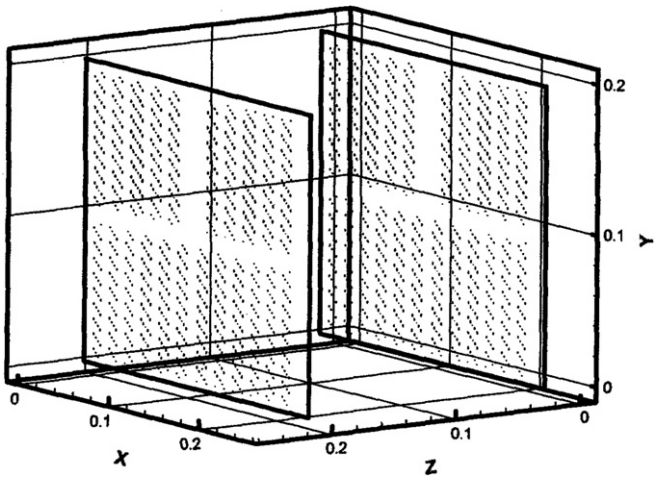

Fig. 17. **V** vectors for the L12W5H1 hollow clay brick ($z = 0.02$ and $z = 0.21$).

number and its arrangement at four indoor–outdoor temperature differences, with or without the hole surface radiation being taken into account. Following conclusions may be obtained.

1. The enhanced influence of radiation heat transfer on the equivalent thermal conductivity depends on the hole number and its arrangement. Generally speaking, the more hole number, the smaller the radiation influence, with the relative enhancement ranging from 23.7% to 3.8%.
2. The equivalent thermal conductivity depends on three heat transfer processes, namely, the natural convection within enclosures, the radiation between hole surfaces and the heat conduction through the solid clay. With the increase in hole numbers, generally the natural convection and the surface radiation will be deteriorated in some extent because of the increased thermal radiation shield or space limitation for the developing of natural convection. However, the increase in holes leads to the increase of heat conduction area in solids with higher thermal conductivity. The final outcome depends on which factor is dominated. The first increase then decrease variation pattern of λ_{rad} with the hole number can be explained from the above understanding.
3. For the 50 kinds of hole configuration at the four indoor–outdoor temperature differences, the configuration of L5W4H1 can be regarded as the optimum, which not only has the lowest equivalent thermal conductivity at standard temperature difference, but also can keep its best isolation character insensitive to the temperature difference. This lowest equivalent thermal conductivity is 0.419 W/(m K), which is only 53.1% of the solid clay. Thus adoption of such multi-holed clay brick for wall construction can make a significant energy-saving for buildings.
4. From engineering point of view, when the hole number in length varies from 4 to 8 and the hole number in width varies from 2 to 5, the values of the equivalent thermal conductivity of the hollow clay brick walls have only slight change. From the view of reducing clay consumption, the hollow clay bricks in use can adopt larger void fraction.
5. The indoor–outdoor temperature difference has a positive effect of the equivalent thermal conductivity. However, in most cases there is only a change of no more than 5%, especially for the optimum configuration such variation can be neglected. Therefore, if the adopted configuration is the optimum or near the optimum, the equivalent thermal conductivity can be taken as constant for whatever indoor–outdoor design temperatures.
6. The flow fields and temperature distributions of air in the enclosures are more or less like those of the benchmark problem (natural convection in a square cavity). With the increase in holes, the natural convection is deteriorated and the radiation is reduced. And the configuration with 60 holes the air temperature isothermals are almost parallel to each other, showing conduction dominated heat transfer process.

Acknowledgements

This work is supported by National Fundamental Key Project of R&D of China (2007CB206902) and the National Natural Science Foundation of China (50636050).

References

[1] O. Laguerre, D. Flick, Heat transfer by natural convection in domestic refrigerators, J. Food Eng. 62 (2004) 79–88.
[2] G. Lauriat, G. Desrayaud, Effect of surface radiation on conjugate natural convection in partially open enclosures, Int. J. Therm. Sci. 45 (2006) 335–346.
[3] H. Bouali, A. Mezrhab, H. Amaoui, M. Bouzidi, Radiation-natural convection heat transfer in an inclined rectangular enclosure, Int. J. Therm. Sci. 45 (2006) 553–566.
[4] N. Ramesh, W. Merzkirch, Combined convective and radiative heat transfer in side-vented open cavities, Int. J. Heat Fluid Flow 22 (2001) 180–187.
[5] K.A.R. Ismail, J.R. Henriquez, Two-dimensional model for the double glass naturally ventilated window, Int. J. Heat Mass Transfer 48 (2005) 461–475.
[6] H.B. Awbi, A. Hatton, Natural convection from heated room surfaces, Energy Build. 30 (1999) 233–244.
[7] S. Ergin, Surface radiation with conduction and natural convection in a two-floor enclosure, Energy Build. 32 (2000) 57–70.
[8] Frank P. Incropera, David P. DeWitt, Introduction to Heat Transfer, fifth ed., John Wiley & Sons, New York, 2003.
[9] C.Y. Zhao, W.Q. Tao, Natural convections in conjugated single and double enclosures, Int. J. Heat Mass Transfer 30 (1995) 175–182.
[10] S. Lorente, M. Petit, R. Javelas, Simplified analytical model for thermal transfer in vertical hollow brick, Energy Build. 24 (1996) 95–103.
[11] S. Lorente, M. Petit, R. Javelas, The effects of temperature conditions on the thermal resistance of walls made with different shapes vertical hollow bricks, Energy Build. 28 (1998) 237–240.
[12] S. Castro Cardoso, E. Cheier, Guy Lauriat, Transferts de chaleur dans une structure alveolaire, Thermique et Microtechnologies, Elsevier, Paris, 2003, pp. 507–512.

[13] J.J. del Coz Díaz, P.J. García Nieto, A. Martin, A. Lozano Martinez, C. Betegón, Non-linear thermal analysis of light concrete hollow brick walls by the finite element method and experimental validation, Appl. Therm. Eng. 26 (2006) 777–786.
[14] J.J. del Coz Díaz, P.J. García Nieto, C. Betegón, M.B. Prendes, Analysis and optimization of the heat-insulating light concrete hollow brick walls design by the finite element method, Appl. Therm. Eng. 27 (2007) 1445–1456.
[15] W.Q. Tao, Numerical Heat Transfer, second ed., Xi'an Jiaotong University Press, Xi'an, China, 2001.
[16] Z.Y. Li, W.Q. Tao, A new stability-guaranteed second-order difference scheme, Numer. Heat Transfer B 42 (2002) 349–365.
[17] Z.G. Qu, W.Q. Tao, Y.L. He, Three-dimensional numerical simulation on laminar heat transfer and fluid flow characteristics of strip fin surface with X-arrangement of strips, ASME J. Heat Transfer 126 (2004) 697–707.
[18] G. Barakos, E. Mitsoulis, Natural convection flow in a square cavity revisisted: laminar and turbulent models with wall function, Int. J. Numer. Meth. Fluids 18 (1994) 695–719.